The Nondimensional Scaling of Turbulence Characteristics and Turbulent Diffusivity

G.R. McKee,[1] C.C. Petty,[2] R.E. Waltz,[2] C. Fenzi,[1] R.J. Fonck,[1] K.H. Burrell,[2] D.R. Baker,[2] E.J. Doyle,[3] X. Garbet,[4] J.E. Kinsey,[5] T.C. Luce,[2] R.A. Moyer,[6] C.L. Rettig,[3] T.L. Rhodes,[3] D.R. Ross,[7] G.M. Staebler,[2] R. Sydora,[8] M.R. Wade[9]

[1]University of Wisconsin-Madison, Madison, WI, United States of America
[2]General Atomics, San Diego, California, USA
[3]University of California, Los Angeles, California, USA
[4]Association Euratom-CEA sur la Fusion, Cadarache, France
[5]Lehigh University, Bethlehem, Pennsylvania, USA
[6]University of California, San Diego, California, USA
[7]University of Texas-Austin, Austin, Texas, USA
[8]University of Alberta, Edmonton, Alberta, Canada
[9]Oak Ridge National Laboratory, Oak Ridge, Tennessee, USA

email contact of main author: mckee@fusion.gat.com

Abstract. Plasma turbulence characteristics, including radial correlation lengths, decorrelation times, amplitude profile, and flow velocity, have been measured during a ρ^* scan on DIII–D while all other transport-relevant dimensionless quantities (β, ν^*, κ, q, T_e/T_i...) are held nearly constant. The turbulence is measured by examining the correlation properties of the local long-wavelength ($k_\perp \rho_I \leq 1$) density fluctuations, measured with beam emission spectroscopy. The radial correlation length of the turbulence, $L_{c,r}$, is shown to scale with the local ion gyroradius, with $L_{c,r} \approx 5\rho_I$, while the decorrelation times scale with the local acoustic velocity as $\tau_c \sim a/c_s$. The turbulent diffusivity parameter, $D \sim (L_{c,r}^2/\tau_c)$, scales in a roughly gyro-Bohm-like fashion, as predicted by the gyrokinetic equations governing turbulent transport. The experimental one-fluid power balance heat diffusivity scaling and that from GLF23 modeling compare reasonably well.

1. Introduction

Transport of energy and particles across confining magnetic field surfaces is observed in most confinement regimes to be anomalously large, i.e, well above predictions from binary Coulomb collisions between plasma ions and electrons (neoclassical transport). This anomalous transport is believed to result from turbulence driven largely by pressure gradients. Predicting the magnitude of this anomalous transport in larger experimental devices has been addressed by applying the nondimensional scaling technique in existing tokamaks [1-5]. A central assumption in the nondimensional scaling approach is that this anomalous transport is a function of local dimensionless quantities, including β (ratio of plasma to magnetic pressure), q (safety factor), ν^* (collisionality), T_e/T_i, κ (elongation), R/a (aspect ratio), L_n/a, L_T/a (density and temperature gradient scale lengths), M (Mach number, $M = v_\phi/c_s$, $c_s = \sqrt{T_e/M_I}$, the sound speed) and ρ^* ($=\rho_I/a$), the ratio of ion gyroradius to plasma minor radius. Existing experimental devices can match all of these transport-relevant dimensionless parameters expected in reactor scale devices with the exception of ρ^*, thus the scaling of transport with ρ^* is of central importance.

Significant experimental and theoretical effort has been expended on determining the ρ^* scaling of anomalous transport. Nearly all theories of turbulent transport are inherently gyro-Bohm and thus predict that $\chi \sim \chi_B(\rho^*)^1$, with $\chi_B = \rho_s c_s$. Experiments, however, have shown that transport coefficients can scale in a gyroBohm or Bohm-like fashion, depending on the plasma confinement regime (L– or H–mode) and the transport channel under investigation [5-7]. The ion channel in L–mode plasmas typically exhibits a Bohm or worse-than-Bohm like scaling, $\chi_I \sim \chi_B(\rho^*)^0$, as can the global energy confinement scaling. Electron heat transport, in contrast, is always observed to exhibit gyro-Bohm like scaling. The effective heat diffusivity and global energy confinement scaling can then depend on whether the electron or ion conductivity is dominant.

Previous experimental studies on the nondimensional scaling of transport have been based largely on the scaling of inferred heat and particle transport coefficients and energy confinement times. Typically, one dimensionless parameter, often ρ*, is varied while other dimensionless quantities are held constant. This study represents the first experiment to systematically measure the scaling characteristics of the underlying turbulence driving the anomalous transport during a nondimensional ρ* scan. The goal has been to elucidate the underlying processes and the inherent turbulence scaling? These experiments were performed in the DIII–D tokamak, and the turbulence was characterized by measuring density fluctuations with the beam emission spectroscopy diagnostic system [8,9]. The experiments, fluctuation measurements, and implications are discussed.

2. ρ* Scaling Experiments

In order to determine the ρ* scaling of plasma turbulence structures and parameters, plasma discharges with well matched dimensionless quantities ($\beta, \nu^*, q, T_e/T_i$, M...) were produced while ρ* was varied. The discharges were elliptical and inner wall limited L–mode plasmas. These were chosen to provide relatively quiescent, steady-state plasma conditions that are preferable for fluctuation diagnosis. The plasma geometry was maintained constant during the scan with major radius R_o=1.65 m, minor radius a=0.63 m, and elongation κ=1.54.

The ρ* scan was performed by varying the toroidal magnetic field and current (to match q) by a factor of 2, as has been the standard method in previous nondimensional scaling experiments on DIII–D [6]. Density and heating power are adjusted via gas puffing and neutral beam power as necessary to keep the profiles of all dimensionless parameters, with the exception of ρ*, constant. The resulting temperature and field variation changes ρ* by a factor of roughly 1.6 in this scan. The profiles of ρ*, β, ν*, q, T_e/T_i and M are shown in Fig. 1, indicating the roughly 1.6 variation of ρ* while other dimensionless variables are held nearly constant across the plasma profile. A slight mismatch in the Mach number will be discussed in a later section. The energy confinement time for the high and low-ρ* discharges varies from 47 to 60 ms, and thus exhibited Bohm like scaling ($\tau_E \propto B^{1/3}$).

The linear gyrokinetic ballooning mode growth rates were calculated for the two discharge conditions in this ρ* scan to determine if the growth rates are well matched. These calculations were performed with the Gyrokinetic simulation (GKS) code [10,11] including actual plasma geometry. The profiles of the maximum linear growth rates normalized to c_s/a are shown in Fig. 2. The very close match between the two curves shows that the discharges

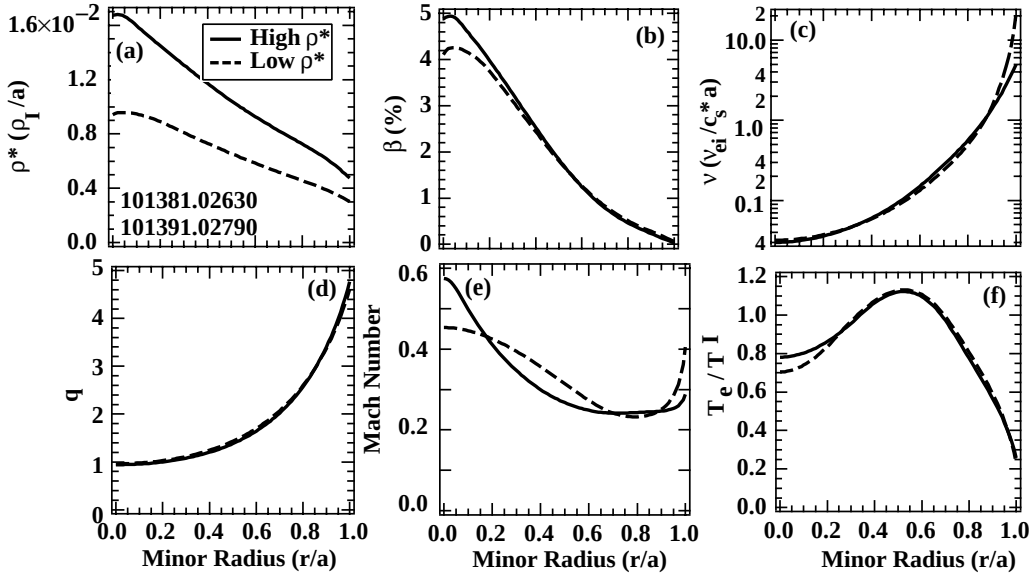

FIG. 1. Profiles of (a) ρ, (b) beta, (c) collisionality, and (d) safety factor q, (e) Mach number, (f), T_e/T_i ratio for the dimensionless ρ* scan. ρ* is varied by 1.6 while other quantities are held nearly constant.*

are well matched theoretically since these rates depend on all dimensionless parameters except ρ*.

3. Fluctuation Parameter Scaling

Measuring the scaling of the radial correlation length, decorrelation time and amplitude of turbulent eddy structures was the primary goal of this study. Measurements of these fluctuation characteristics, as well as their scaling, were obtained with the beam emission spectroscopy (BES) diagnostic. The BES system measures the local long wavelength ($k_\perp \le 2.5$ cm^{-1}) density fluctuations at a spatial resolution of $\Delta r \approx 1$ cm. It observes the Doppler-shifted neutral beam emission at D_α (n=3-2 at λ~653 nm) arising from excitation of the beam as it traverses the plasma and collides with the background plasma ions and electrons. Diagnostic details are discussed in Ref. [8]. The long wavelength density fluctuations measured are believed to arise predominantly from electrostatic drift-wave like turbulence and can transport ions and electrons across magnetic field via turbulent E×B diffusion: $\Gamma = \langle \tilde{n}\tilde{v}_r \rangle = \langle \tilde{n}\tilde{E}_\theta / B_T \rangle$.

The BES instrument has 32 spatial channels which were deployed as follows: 14 radially separated channels and two poloidal arrays of 8 channels each, with a roughly 1 cm. separation between radial and poloidal channels. The setup is shown in Fig. 3 along with an equilibrium reconstruction of the flux surface shapes. Two channels are situated deeper in the plasma to monitor common mode fluctuation power [9]. The radially separated channels allow for a measurement of the radial correlation length and fluctuation amplitude profile, while the poloidally separated channels provide measurements of the decorrelation time, poloidal correlation length, and poloidal convection velocity of the density fluctuations, all quantities integral to this investigation.

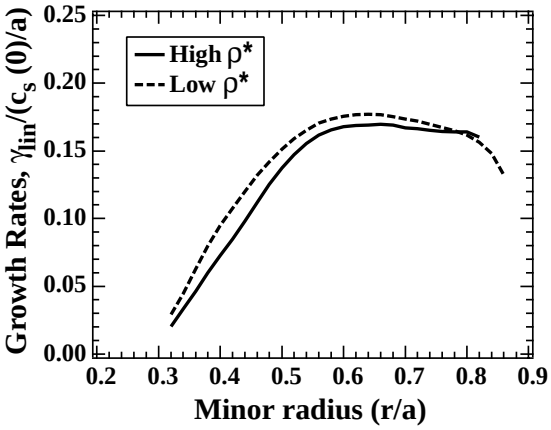

FIG. 2. Profiles of the maximum linear growth rate (calculated with the GKS code), normalized to $c_S(0)/a$, in the low and high ρ discharges, showing a very close match indicating that turbulent transport would be expected to be gyroBohm like.*

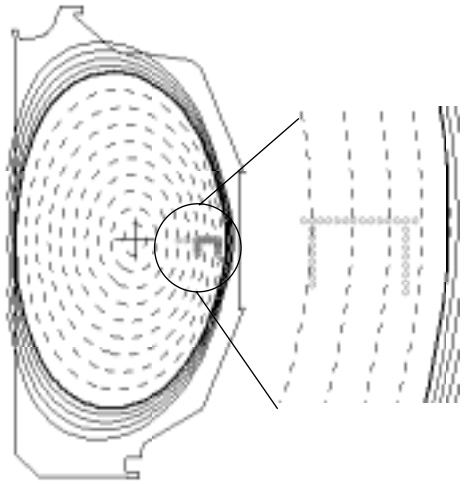

FIG. 3. EFIT equilibrium reconstruction showing the locations of the 32 spatial BES channels, with one radial array (14 channels), 2 poloidal arrays (8 channels each) and 2 common mode monitoring channels. The array was moved on repeat discharges to scan across the profile.

A. Fluctuation amplitude profile

The fluctuation amplitude profiles, shown in Fig. 4(a), indicate that the normalized fluctuation level, ñ/n, increases over the entire profile with ρ*. The profiles show that in both ρ* conditions, the fluctuation amplitude increases rapidly from the core to the edge of the plasma. This presents a practical issue in that measurement of quantities such as correlation lengths and decorrelation times requires sufficient signal to noise in the fluctuation amplitude. As ñ/n falls below about 0.5%, the signal-to-noise becomes too low to confidently measure the quantities. Thus the turbulence characteristics are studied in the radial region $0.7 \le \rho \le 1.0$ where sufficient signal-to-noise allows for such measurements. The ratio of the fluctuation profiles, $[\tilde{n}/n]_{2\,T}/[\tilde{n}/n]_{1\,T}$, is shown in Fig. 4(b) indicating a scaling of roughly $\tilde{n}/n \sim (\rho^*)^{1.4\pm0.4}$. GyroBohm based models predict that the fluctuation amplitude should scale as

$\tilde{n}/n \sim (\rho^*)^1$ [12,13]. The radial variation of the $\tilde{n}/n$ ratio shows significant variance and, given the experimental uncertainty, is not inconsistent with the gyroBohm predictions.

B. Correlation Lengths

Turbulent eddy structure sizes and their ρ^* scaling are a key property of the turbulence and specific predictions for their magnitude are provided by transport simulations. The BES data provides a direct measure of both the radial and poloidal correlation lengths of the plasma turbulence. These quantities are measured by calculating the ensemble-averaged temporal correlation between nearby spatial channels. These correlation lengths are interpreted as eddy structure sizes in the associated direction (radial or poloidal).

The radial correlation function for the low and high ρ^* conditions at ρ=0.78 are shown in Fig. 5(a). The radial correlation length is taken as the distance over which the correlation has dropped to 1/e. The finite spatial resolution of the BES diagnostic has been spatially deconvolved from the correlation function. For these discharges, the radial correlation lengths at ρ = 0.78 are about 1.6 and 2.4 cm in the low and high ρ^* conditions, respectively. The profile of the correlation length normalized to the ion gyroradii is shown in Fig. 5(b). The radial correlation lengths scale very closely with the local ion gyroradius in both cases such that $L_{c,r} \approx 5\ \rho_I$. These measurements demonstrate that the turbulence radial correlation length scales with the local ion gyroradius and not with the system size of the plasma, which is of course fixed in these experiments. Thus the correlation lengths appear consistent with gyroBohm scaling.

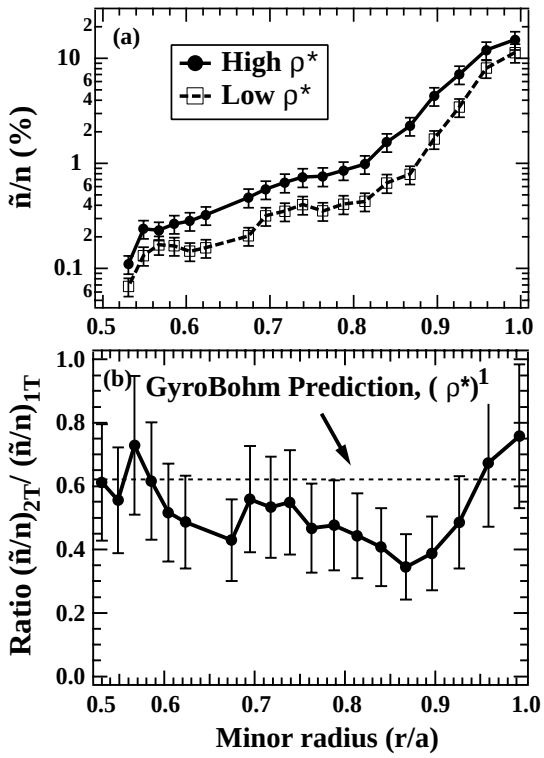

FIG. 4. (a) Profile of the normalized density fluctuation amplitude, ñ/n for the two ρ^* discharges showing a strong radial dependence (note logarithmic scale), (b) ratio of the density fluctuation profile along with a line at 0.6 indicating gyroBohm like predictions.

The radial and poloidal wavenumber spectra are shown in Fig. 6(a) and (b). These spectra demonstrate the self-similar nature of the wavenumber spectra and indicate that beyond just the matching of correlation lengths, an average parameter of the distribution, the distribution of fluctuation power is similar when shown versus normalized wavenumber, $k_\perp \rho_s$. There is a slight shift in the poloidal spectrum between the low and high ρ^* conditions which reflects that the poloidal correlation length does not scale quite as strongly with ρ^* as the radial correlation length. The radial correlation length is the step-size for random-walk diffusion and is thus the quantity that is directly relevant to turbulent transport.

C. Decorrelation times

Eddy decorrelation times, τ_c, the inverse of the k-averaged nonlinear growth rate, also interpreted as eddy turn-over times, are estimated from the experimental BES data as the decorrelation time of the density fluctuations. This quantity is derived from the ensemble averaged temporal correlation functions of poloidally separated channels. Turbulent eddies are typically advecting uniformly in the poloidal direction at or near the local $E_r \times B$ velocity. We use this aspect to convert poloidal correlation functions to a decorrelation time. Temporal cross correlation functions are evaluated between a reference channel, which is typically taken at the base of a poloidal array of BES channels. A temporal correlation function is constructed by graphing the maximum correlation value versus the time delay at which the peak occurs for each of the 9 channels in a poloidal array [9].

Decorrelation functions for the low and high ρ* conditions are shown in Fig. 7(a). It is seen that τ_c increases from about 8 μs at low ρ* to about 11 μs at high ρ*. Figure 8(b) shows this data correctly normalized to a/c_s, a natural time scale from the gyrokinetic equations. The striking feature is that with this normalization, the two profiles match very well, and have a ratio of order unity. There is a slight decrease in this ratio with radius, however the agreement of these quantities between the two ρ* conditions suggests that a/c_s is a proper normalizing parameter and that the decorrelation time exhibits a gyroBohm-like scaling.

D. Turbulent diffusivity scaling

A turbulent diffusivity parameter is constructed from a random walk model of turbulent diffusion, whereby particles are mixed over a radial correlation length on the time scale of a decorrelation time, $D \approx L_{c,r}^2/\tau_c$. The ratio of this diffusivity parameter for the low and high ρ* conditions, calculated from the above measurements, is shown in Fig. 8, along with expectations from a Bohm or gyroBohm like scaling laws. Except for the radially outermost point, which appears

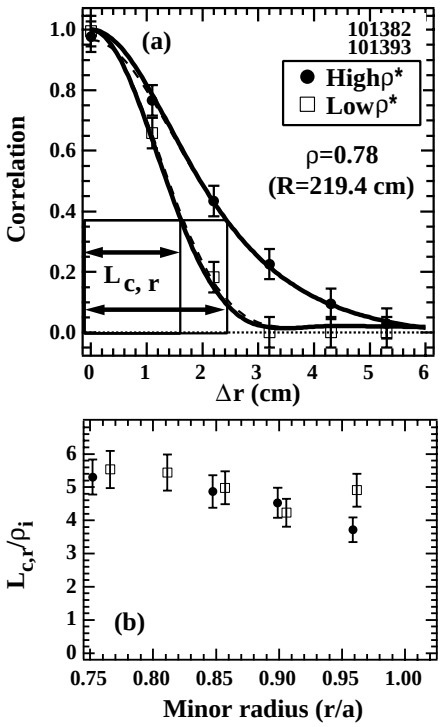

FIG. 5. (a) Radial correlation function at r=0.78 for the two ρ discharges showing shorter radial correlation length ($L_{c,r}$) in low-ρ* discharge, and (b) ratio of the radial correlation length profile to the ion gyroradius showing close scaling of the two ρ* cases, with $L_{c,r} \approx 5\rho_I$.*

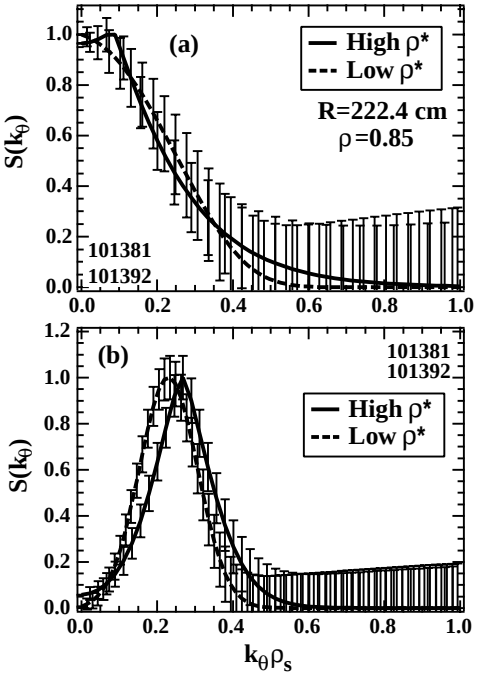

FIG. 6. (a) Comparison of the radial wavenumber spectra in the two conditions showing the self-similar nature, and (b) comparison of the poloidal wavenumber spectra. A slight shift is observed, though this is not believed to be correlated directly with cross-field transport.

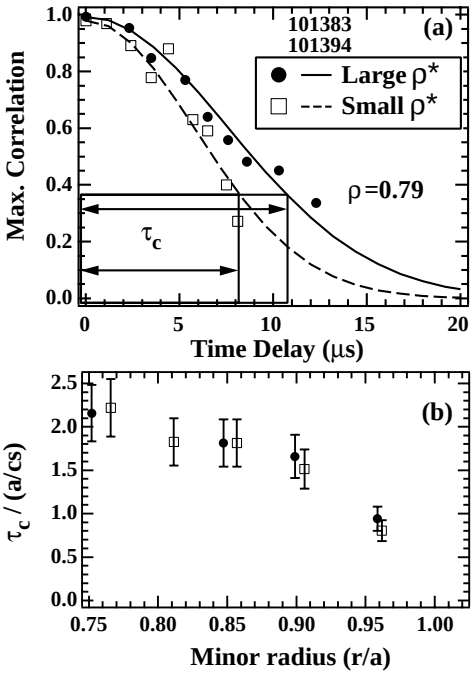

FIG. 7. (a) Temporal correlation function of turbulence at r=0.79 showing increase in decorrelation time from $\tau_c \approx 8$ to $\tau_c \approx 11$ μs as ρ is in increased. Profile of τ_c normalized to a/c_s showing match between the two conditions, indicating a gyroBohm scaling.*

anomalous, the turbulent diffusivity scaling is between the Bohm and gyroBohm conditions, but closer to gyroBohm, as would be expected since both the radial correlation length and decorrelation times scale in a roughly gyroBohm like fashion. The worse-than-Bohm scaling of the edge point (at ρ=0.96) results primarily from the short measured radial correlation length [Fig. 5(b)]. The near edge turbulence has a distinctly different character than the core turbulence which is briefly discussed in the next section. It is noted that it is not the absolute magnitude of the diffusion parameter, but rather the scaling of this quantity that is important for addressing the scaling properties.

E. Flow velocity profile

Turbulent structures advect poloidally in the laboratory frame at a velocity that is the sum of the E×B velocity and a fraction of the ion or electron diamagnetic velocity corresponding to the intrinsic mode phase velocity. Typically the E×B velocity is much larger than diamagnetic velocities so within error bars, the E×B velocity is observed. This velocity is measured experimentally with the poloidal correlation functions discussed in Section 3.C, and is simply $v_{group}=\Delta z/\Delta t$, with Δz the spatial separation and Δt the time delay of the maximum correlation. This is thus a k-averaged group velocity, but the phase shift of poloidal coherency spectra typically show a linear relation, indicating that all wavenumbers are being uniformly advected in the lab frame, or that the derived velocity is nearly the same for all wavenumbers.

The poloidal flow velocity profile is shown in Fig. 10. The fluctuation convection velocity scales closely with the Mach number, $M=v_{tor}/c_s$ away from the edge. However, near the edge region, at $\rho\approx0.96$ in the high ρ^* condition, the fluctuation spectra indicate two distinct modes that are counter propagating, with low-frequency modes traveling in the ion diamagnetic direction, and higher frequency modes propagating in the electron direction. Thus the velocity profile is double-valued for high ρ^* at this location. Dual mode edge urbulence has been observed previously [14] and was interpreted as the observation of distinct electron and ion modes. Here they are presented as characteristics of the edge turbulence, though it

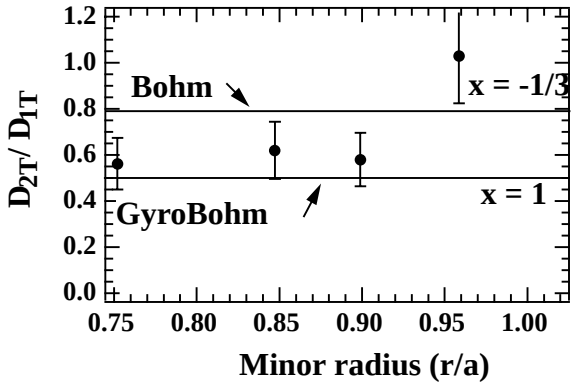

FIG. 8. Ratio of turbulent diffusivity, defined as $D=(L_{c,r})^2/\tau_c$, for the two ρ^* discharges. The profile is most consistent with a gyroBohm like scaling, as expected since both the radial correlation length and decorrelation time scale in a gyroBohm fashion. The anomalously large edge point is discussed in the text.

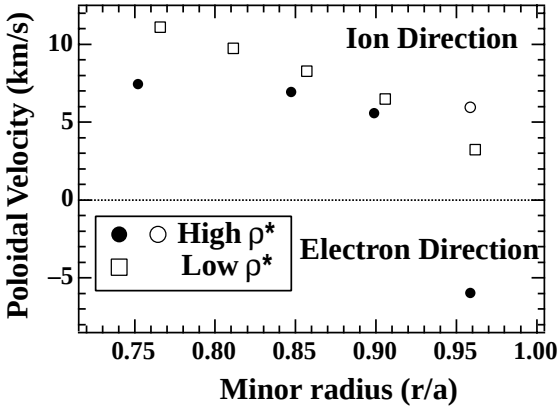

FIG. 9. Profile of the poloidal propagation velocity of the turbulent structures as measured in the lab frame. For the edgemost measurement, two modes are observed in the fluctuation spectra showing an ion and electron mode, both shown.

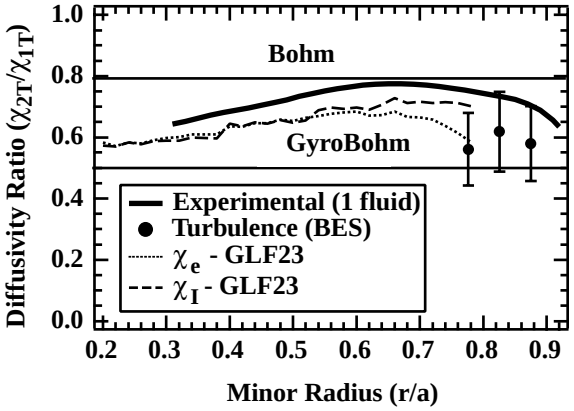

FIG. 10. Profiles of the ratio of heat diffusivity for a one-fluid power balance, GLF23 simulation, and the fluctuation diffusivity parameter showing reasonable consistency.

is not clear if or how they affect confinement. The radial correlation length at this edge location in the high ρ* condition was observed to be well below the scaling curve [Fig. 5(b)] for the other channels suggesting that this edge turbulence has a fundamentally different nature.

4. Modeling Predictions and Discussion

Turbulent transport simulations of these ρ* scaling discharges using the GLF23 model [15] were performed to further elucidate these experimental observations. The GLF23 simulations indicate that ratio of the effective power balance diffusivity scales between Bohm and gyro-Bohm for this pair of ρ* conditions, as shown in Fig. 10. Here we compare the ratio of the effective thermal diffusivities from GLF23 and from the experimental heat flux, as well as that from the turbulence measurements. Within their respective uncertainties, they all roughly agree and indicate that the scaling is between gyro-Bohm and Bohm.

The GLF23 transport model is an intrinsically gyro-Bohm model, and so it is important to identify the gyro-Bohm breaking mechanism in the simulation for these discharges. Gyro-Bohm breaking mechanisms may include small but important mismatches in the dimensionless parameter profiles, nonlinear coupling of highly unstable short wavelength modes to longer wavelength modes that scale with gradient scale lengths (and therefore system sizes) [16-19], or a diamagnetically-driven (ρ*-dependent) ExB shear reduction of growth rates [20]. GLF23 modeling indicates that a slight mismatch in the Mach number (see Fig. 1(f)) may alter the ExB shear rate and break the intrinsic gyro-Bohm scaling of the transport. The E×B shearing rate modifies the growth rate as $\gamma_{NET} = \gamma_{lin} - \gamma_{E\times B}$. $\gamma_{E\times B}$ contains a rotational and diamagnetic term. The simulation showed that the diamagnetic term is negligible and so $\gamma_{E\times B}$ is dominated by the toroidal rotation term. Here, ExB shear effects were found to be more important for the high r* case resulting in the apparent worse than gyro-Bohm scaling.

We note that with a two-fluid power balance analysis applied to these discharges, the electron heat diffusivity (χ_e) scales in a gyro-Bohm like fashion while the ion heat diffusivity (χ_I) scales worse-than-Bohm, as has been seen in past experiments [6]. These recent experimental results do not resolve this issue. Further simulations and experiments are required to understand this observation. Present studies suggest that the worse-than-Bohm ion diffusivity may be related to the difference between the power balance diffusivity and the incremental diffusivity. Small changes in the critical gradient, induced by slight Mach number mismatches, can lead to large changes in the predicted heat flux, thus allowing for corresponding differences in the scaling characteristics of the incremental and power-balance heat diffusivities. This will be investigated in future studies.

5. Conclusion

This experimental study has provided the first direct measurements of the scaling of density fluctuation characteristics during a systematic nondimensional ρ* scan. These measurements were obtained with the BES diagnostic in well-matched L–mode discharges on DIII–D where all dimensionless parameters, with the exception of ρ*, are held constant. It has been shown that the turbulence radial correlation lengths scales with the local ion gyroradius, ρ_I, and that the decorrelation times, τ_c, scales with a/c_s. The fluctuation amplitude scales as $\tilde{n}/n \propto (\rho^*)^{1.4\pm0.4}$. These scaling characteristics are in reasonably good agreement with predictions from gyro-Bohm models of turbulent transport. The turbulent diffusivity parameter ($D \approx L_{c,r}^2/\tau_c$) scales between gyro-Bohm and Bohm-like, but appears closer to gyro-Bohm. Within the uncertainties, this agrees with the single-fluid experimental power balance heat diffusivity scaling, and that from the GLF23 modeling.

Acknowledgment

Work supported by U.S. Department of Energy under Grant Nos. DE-FG03-96ER54373, DE-FG03-95ER54294, DE-FG03-86ER53225, and Contracts DE-AC03-99ER54463 and DE-AC05-96OR22464.

References

[1] WALTZ, R.E., DeBOO, J.C., ROSENBLUTH, M.N., Phys. Rev. Lett. **65**, 2390 (1990).
[2] CONNOR, J.W., TAYLOR, J.B., Nucl. Fusion **17**, 1047 (1977).
[3] CORDEY, J.G., BALET, B., CAMPBELL, D. *et al.*, Plasma Phys. Control. Fusion **38**, A67 (1996).
[4] PERKINS, F.W., BARNES, C.W., JOHNSON, D.W. *et al.*, Phys. Fluids B **5**, 477 (1993).
[5] PETTY, C.C., LUCE, T.C., PINSKER, R.I. *et al.*, Phys. Rev. Lett. **74**, 1763 (1995).
[6] PETTY, C.C., LUCE, T.C., BURRELL, K.H. *et al.*, Phys. Plasmas **2**, 2342 (1995).
[7] LUCE, T.C, PETTY, C.C., BALET, B., CORDEY, J.G., IAEA-1996, F1-CN-64/AP1-3.
[8] McKEE, G.R., ASHLEY, R., DURST, R., FONCK, R., et al., Rev. Sci. Instrum. **70**, 913 (1999).
[9] DURST, R.D., FONCK, R.J., COSBY, G. *et al.*, Rev. Sci. Instrum. **63**, 4907 (1992).
[10] KOTSCHENREUTHER, M. *et al.*, Comput. Phys. Commun. **88**, 128 (1995).
[11] WALTZ, R.E., MILLER, R.L., Phys. Plasmas **6**, 4264 (1999).
[12] MANFREDI, G., OTTAVIANI, M., Phys. Rev. Lett. **79**, 4190 (1997).
[13] ROSS, D.W., private communication.
[14] DURST, R.D., FONCK, R.J., J.S. Kim *et al.*, Phys. Rev. Lett. **71**, 3135 (1993).
[15] Waltz, R.E., Staebler, G.M., Dorland, W. *et al*., Phys. Plasmas **4**, 2482 (1997).
[16] SYDORA, R.D., DECYK, V.K., DAWSON, J.M., Plasma PHys. Control. Fusion **38**, A281 (1996).
[17] BIGLARI, H., DIAMOND, P.H., Phys. Fluids B **3**, 1797 (1991).
[18] TANG, W.M., REWOLDT, G., Phys. Fluids B **5**, 2451 (1993).
[19] FURNISH, G., HORTON, W., KISHIMOTO, Y. *et al*., Phys. Plasmas **4**, 169 (1997).
[20] GARBET, X., WALTZ, R.E., Phys. Plasmas **3**, 1898 (1996).